Homeologs of the *Nicotiana benthamiana* Antiviral ARGONAUTE1 Show Different Susceptibilities to microRNA168-Mediated Control[1][OPEN]

Torsten Gursinsky[2], Walter Pirovano[2], Giorgio Gambino, Susann Friedrich, Sven-Erik Behrens, and Vitantonio Pantaleo*

Institute of Biochemistry and Biotechnology, Martin Luther University Halle-Wittenberg, D–06120 Halle/Saale, Germany (T.G., S.F., S.-E.B.); BaseClear, 233CC Leiden, The Netherlands (W.P.); Institute for Sustainable Plant Protection-Consiglio Nazionale delle Ricerche, Research Unit of Grugliasco, 10135 Turin, Italy (G.G.); and Institute for Sustainable Plant Protection-Consiglio Nazionale delle Ricerche, Research Unit of Bari, 70126 Bari, Italy (V.P.)

ORCID IDs: 0000-0002-2717-4735 (W.P.); 0000-0001-6677-6504 (V.P.).

The plant ARGONAUTE1 protein (AGO1) is a central functional component of the posttranscriptional regulation of gene expression and the RNA silencing-based antiviral defense. By genomic and molecular approaches, we here reveal the presence of two homeologs of the *AGO1*-like gene in *Nicotiana benthamiana*, *NbAGO1-1H* and *NbAGO1-1L*. Both homeologs retain the capacity to transcribe messenger RNAs (mRNAs), which mainly differ in one 18-nucleotide insertion/deletion (indel). The indel does not modify the frame of the open reading frame, and it is located eight nucleotides upstream of the target site of a microRNA, miR168, which is an important modulator of AGO1 expression. We demonstrate that there is a differential accumulation of the two *NbAGO1-1* homeolog mRNAs at conditions where miR168 is up-regulated, such as during a tombusvirus infection. The data reported suggest that the indel affects the miR168-guided regulation of *NbAGO1* mRNA. The two AGO1 homeologs show full functionality in reconstituted, catalytically active RNA-induced silencing complexes following the incorporation of small interfering RNAs. Virus-induced gene silencing experiments suggest a specific involvement of the *NbAGO1* homeologs in symptom development. The results provide an example of the diversity of microRNA target regions in *NbAGO1* homeolog genes, which has important implications for improving resilience measures of the plant during viral infections.

The *ARGONAUTE1* gene (*AGO1*) was first discovered in Arabidopsis (*Arabidopsis thaliana*) and further described trough plant mutants that showed pleiotropic developmental anomalies. Examples of phenotypic traits influenced by AGO1 are cotyledon expansion, leaf polarity, branching of the inflorescence stem, rooting, differentiation of flowers, and fertility (Kidner and Martienssen, 2004, 2005; Vaucheret et al., 2004; Sorin et al., 2005). The pleiotropic character of *AGO1* is determined by the role of the AGO1 protein as a core component of the microRNA (miRNA)/RNA-induced silencing complex (RISC) in posttranscriptional gene silencing (PTGS; Baumberger and Baulcombe, 2005). Most miRNAs are incorporated into AGO1 and guide the RISC to its mRNA target through sequence complementarity; as a result, the mRNA translation is inhibited by endonucleolytic cleavage or other yet incompletely characterized mechanisms (Brodersen et al., 2008; Lanet et al., 2009; Iwakawa and Tomari, 2013). Beside its role in PTGS and in concert with other proteins of the Argonaute clade, AGO1 plays a key role in the RNA silencing-based antiviral defense (Takeda et al., 2008; Harvey et al., 2011; Scholthof et al., 2011a; Wang et al., 2011); similar to miRNAs, virus-derived small interfering RNAs (vsiRNAs) are incorporated into AGO1-containing RISC, leading to the inactivation of viral RNAs by cleavage. In turn, viruses may encode viral suppressors that impair AGO1 functionality (for review, see Burgyán and Havelda, 2011).

AGO1 homeostasis is in part coordinated through a feedback mechanism. Thus, microRNA168 (miR168)-guided cleavage of *AGO1* mRNA was demonstrated to ensure an optimal balance of miRNA steady-state levels (Vaucheret et al., 2004, 2006; Vazquez et al.,

[1] This work was supported by the Italian Ministry of Economy and Finance through the Consiglio Nazionale delle Ricerche (CNR; grant no. C.I.S.I.A. Legge 191/2009 and by the AQUA project), by the Dipartimento Agro-Alimentare-CNR (to V.P.), by a CNR Short Term Mobility Grant 2014 (to V.P.), and by the Deutsche Forschungsgemeinschaft (grant no. BE1885/7–2, project B6 of the Research Training Group 1591, and project A7 of the Collaborative Research Center 648 to T.G., S.F., and S.-E.B.) at Martin Luther University Halle-Wittenberg.

[2] These authors contributed equally to the article.

* Address correspondence to vitantonio.pantaleo@cnr.it.

The author responsible for distribution of materials integral to the findings presented in this article in accordance with the policy described in the Instructions for Authors (www.plantphysiol.org) is: Vitantonio Pantaleo (vitantonio.pantaleo@cnr.it).

T.G., G.G., S.F., and V.P. performed the experiments; W.P. performed the bioinformatics analysis; S.-E. B. and V.P. wrote the article; V.P. conceived the original research plan.

[OPEN] Articles can be viewed without a subscription.

www.plantphysiol.org/cgi/doi/10.1104/pp.15.00070

2004; Vaucheret, 2009). Conversely, overexpression of miR168 (e.g. in plants expressing miR168 under the control of the 35S promoter) is accompanied by a decrease in *AGO1* mRNA accumulation, and it is associated with the cleavage of *AGO1* mRNA. Moreover, miR168 also overaccumulates in plants that express a miR168-resistent *AGO1* mRNA (i.e. 4m-AGO1), owing to stabilization by AGO1 (Vaucheret et al., 2004, 2006).

Nicotiana benthamiana is one of the most widely used models to study RNA virus-plant interactions. Upon infection, *N. benthamiana* activates and orchestrates an antiviral RNA interference response, which mostly parallels the RNA interference pathways that were described for the model plant Arabidopsis (Qiu et al., 2002; Omarov et al., 2006; Pantaleo et al., 2007; Goodin et al., 2008; Csorba et al., 2009; Várallyay et al., 2010; Scholthof et al., 2011a, 2011b). The recent release of the draft genome sequence of *N. benthamiana* provides the opportunity to shed new light on additional layers of plant-virus interaction, because *N. benthamiana* is susceptible to a considerably broader spectrum of viruses than Arabidopsis.

Tombusviruses like *Cymbidium ringspot virus* (CymRSV) and *Tomato bushy stunt virus* (TBSV) are well-accepted prototypes to study RNA silencing-based plant-virus interactions. Tombusviruses have a broad host range spanning approximately 20 plant families and approximately 120 species (Yamamura and Scholthof, 2005). The tombusvirus genomic and subgenomic RNAs are substrates of DICERS yielding high levels of viral small interfering RNAs (siRNAs; Szittya et al., 2002, 2010), and these viruses encode a 19-kD protein (P19) that is a potent suppressor of RNA silencing (Voinnet et al., 1999; Vargason et al., 2003). While Arabidopsis is not permissive to a tombusvirus infection, CymRSV and TBSV replicate in heterologous systems such as *Saccharomyces cerevisiae* (Panavas and Nagy, 2003; Pantaleo et al., 2003; Navarro et al., 2006). TBSV also was recently applied in a plant cytoplasm-based system to reproduce viral replication as well as antiviral RNA silencing in vitro (Gursinsky et al., 2009; Schuck et al., 2013).

Nicotiana spp. frequently contain so-called homeologs; these are duplicated genes in the same plant genome derived from different ancestors in polyploidy (Bombarely et al., 2012a). In this report, we show that *N. benthamiana* possesses two *NbAGO1*-like homeolog genes, *NbAGO1-1H* and *NbAGO1-1L*. They differ mainly by one 18-nucleotide-long insertion/deletion (indel), which does not modify the translational frame. Importantly, the indel is located in the immediate vicinity of the miR168 target site, and our data suggest that its presence considerably affects the miR168-guided posttranscriptional regulation of *NbAGO1* mRNA. The indel effect is highlighted under conditions of an increased miR168 accumulation (e.g. during a viral infection). The two NbAGO1 homeologs show full functionality in reconstituted, catalytically active RISC following the incorporation of siRNAs. Moreover, virus-induced gene silencing (VIGS) experiments suggest a specific, redundant involvement of the *NbAGO1* homeologs in susceptibility to viral infection but a divergent involvement in symptom development. The expression of two types of *NbAGO1-1* mRNAs is proposed to represent an evolutionary adaptation to improve resilience measures of the plant during viral infections or other stresses accompanied by miR168 up-regulation.

RESULTS

A New *AGO1* Locus in the *N. benthamiana* Genome

Previously, two *AGO1*-like genes were identified in *N. benthamiana*: *NbAGO1-1* and *NbAGO1-2* (National Center for Biotechnology Information accession nos. DQ321488 and DQ321489, respectively). Both *NbAGO1*-like genes were shown to be required for a full systemic silencing of transgenes, which is in close analogy to observations made with hypomorphic mutants of Arabidopsis *AGO1* alleles (Jones et al., 2006). We retrieved the *NbAGO1* genes from the *N. benthamiana* draft genome available for public research (http://solgenomics.net/organism/Nicotiana_benthamiana/genome) and, unexpectedly, identified an additional *NbAGO1* locus. By comparing the sequence of the second exon, we determined a high similarity with the 5′-terminal sequence of *NbAGO1-1* (DQ321488) but not with *NbAGO1-2* (DQ321489). A pairwise alignment of the known and the newly determined *NbAGO1-1* loci revealed a different length; accordingly, we renamed the two loci as *NbAGO1-1L* (for low) and *NbAGO1-1H* (for high). The *NbAGO1-1L* locus (corresponding to DQ321488) is 7,008 bp long, while the *NbAGO1-1H* locus is 7,195 bp long (introns and exons included but promoter and terminator sequences excluded; Supplemental Fig. S1). Both loci contain 22 exons and 22 introns, and the different length is mainly explained by indels at the intron level (e.g. within intron 11; Fig. 1A; Supplemental Fig. S1).

To validate the gene sequences that were retrieved from the *N. benthamiana* genomic data, we searched for intronic/exonic sequences to design and apply a PCR-based strategy to specifically discriminate between the two *NbAGO1-1* loci. Thus, specific oligonucleotides were designed that annealed exclusively within the *NbAGO1-1H* intron 11 (gray bar in Fig. 1B, top; Supplemental Fig. S2A). We applied a similar approach to the terminator region, where an approximately 300-bp-long indel discriminates the two *NbAGO1-1* loci (gray bar in Fig. 1B, middle; Supplemental Fig. S2B). The obtained PCR products had the expected sizes (PCR amplicons in Fig. 1B, bottom); they were subsequently cloned and sequenced. The obtained sequence data confirmed the *N. benthamiana* draft genome sequence (Bombarely et al., 2012b).

NbAGO1-1L and NbAGO1-1H Are Functional in Generating Transcripts

An 18-nucleotide-long indel located within exon 2 (position 322, referred to as the coding sequence section;

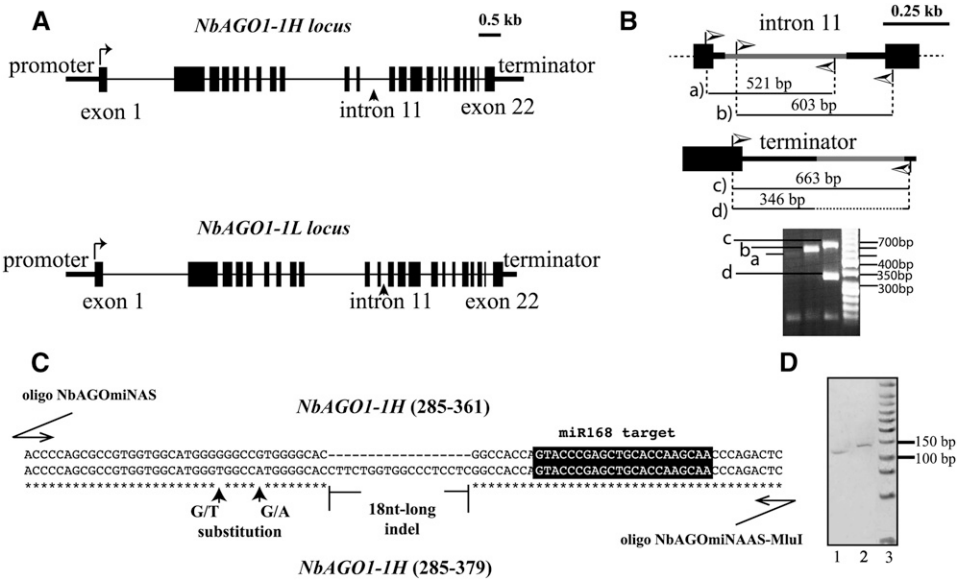

Figure 1. Organization of *NbAGO1-1H* and *NbAGO1-1L* loci. A, Schematic representation of the structures of *NbAGO1-1H* (top) and *NbAGO1-1L* (bottom) loci. Black lines represent introns, vertical bars represent exons, and horizontal bars at the two extremities are untranslated regions. B, Graphic representing the PCR-based approach used to reveal the two alternative *NbAGO1-1* loci in the intron 11 and terminator regions (top and middle, respectively). The high-resolution gel electrophoresis of the PCR products is reported at the bottom. Lowercase letters (i.e. a–d) indicate single amplification products, which are represented as thin black lines at the top and middle. C, Alignment of the section of exon 2 containing the 18-nucleotide-long indel, which was used to reveal the expression of the two *NbAGO1-1* transcripts. The applied oligonucleotides are described in "Materials and Methods." Stars indicate the consensus sequence; black vertical arrows mark two detected nucleotide substitutions. The black box highlights the miR168 target site. D, High-resolution acrylamide gel electrophoresis of the two RT-PCR fragments from the two RNA transcripts described in C. Lanes 1 and 2 show the 129- and 147-bp-long amplicons that were obtained from the *NbAGO1-1L* and *NbAGO1-1H* transcripts, respectively. A low M_r New England Biolabs marker is in lane 3.

Supplemental Fig. S1) was used to detect and discriminate *NbAGO1-1L* and *NbAGO1-1H* transcripts in *N. benthamiana*. First, polyadenylated RNAs were selectively purified from total RNA and randomly reverse transcribed. The complementary DNA (cDNA) was then subjected to PCR using oligonucleotides that were applicable to both transcripts of *NbAGO1-1L* and *NbAGO1-1H* encompassing the 18-nucleotide-long indel (see "Materials and Methods" and alignment in Fig. 1C). The PCR was first analyzed by high-resolution gel electrophoresis. It revealed two main amplicon species, which were gel purified and again resolved by gel electrophoresis. In Figure 1D, ethidium bromide-stained amplicons are shown to have the expected (i.e. based on the retrieved sequence) lengths of 129 bp (from the *NbAGO1-1L* transcript) and 147 bp (from the *NbAGO1-1H* transcript; lanes 1 and 2, respectively). Sanger sequencing of the two amplicons confirmed the presence of both the indel and of certain G/T and T/A polymorphic nucleotides (single-nucleotide polymorphisms; Fig. 1C). The characteristics of both transcripts were further confirmed through the amplification and sequencing of longer segments (data not shown).

Recently, an *N. benthamiana* transcriptome analysis was carried out by RNA deep sequencing and assembly (Nakasugi et al., 2013). The available data set was searched for the *NbAGO1-1* transcripts and, indeed, both species were found. Based on the 18-nucleotide-long indel (Fig. 1C), Nbv3K765634670 is the sole transcript that represents *NbAGO1-1L*, whereas several other transcripts represent *NbAGO1-1H* (i.e. Nbv3K605752598, Nbv3K805664652, Nbv3K705828682, Nbv3K705826800, Nbv3K745621734, and Nbv3K745621399; Supplemental Fig. S3). The study of Nakasugi et al. (2013) did not highlight the presence of the *NbAGO1-1L* transcript (see "Discussion").

The miR168-Guided Silencing Machinery Cleaves NbAGO1-1H and NbAGO1-1L at the Target Site

miR168 is a highly conserved miRNA within the plant kingdom (Supplemental Fig. S4; Cuperus et al., 2011). Accordingly, the miR168 target site is also highly conserved within the annotated *NbAGO1* sequences (Fig. 2A). Both *NbAGO1-1L* and *NbAGO1-1H* possess an identical putative miR168 target site and, notably, the 18-nucleotide-long indel is located only eight nucleotides upstream (Fig. 2A). In order to prove whether miR168 targets and cleaves the *NbAGO1-1* mRNAs in *N. benthamiana*, we performed a 5′-RACE analysis. Ten clones out of 10 sequences confirmed the expected cleavage between nucleotides complementary to positions 10 and 11 of miR168 (Fig. 2B, vertical arrow).

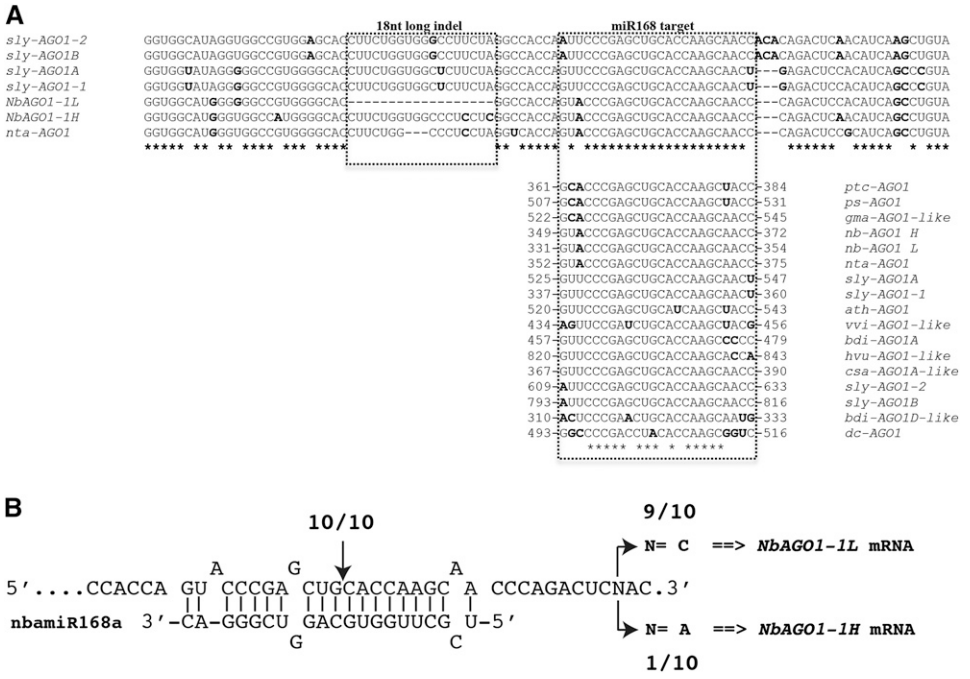

Figure 2. Sequence diversity of the indel-containing region and the miR168 target. A, Sequence diversity of the indel-containing region of all known annotated or predicted *AGO1* mRNAs from plants belonging to the Solanaceae family. Highlighted are the 18-nucleotide-long indel (box on the left) and the miR168 target site (box on the right). In the latter case, the alignment analysis was extended to other plant species. Sequences in boldface are not conserved and show a nucleotide occurrence of less than 50%. B, 5′-RACE analysis of the miR168-mediated cleavage site. The vertical arrow indicates the positions corresponding to the 5′ ends of *NbAGO1-1L* and *NbAGO1-1H* RNAs that were determined by 5′-RACE and the number of 5′-RACE clones corresponding to the site. The single-nucleotide polymorphism (indicated by N) at the 3′ end of the reported sequence was used as a molecular mark to discriminate the cleaved alternative transcript. Accession numbers of retrieved annotated or predicted *AGO1* mRNAs are as follows: ptc, *Populus trichocarpa* (XM002318302); ps, *Pisum sativum* (EF108450); gma, *Glycine max* (XM003548263); nta, *N. tabacum* (AB542739); sly, *S. lycopersicum* (JX467704, JX945381, JX945382, and JX467705); ath, Arabidopsis (NM001198240); vvi, *Vitis vinifera* (XM002271189); bdi, *Brachypodium distachyon* (XM003580292 and XM_003563186); hvu, *Hordeum vulgare* (AK373112); csa, *Cucumis sativus* (XM004137339); and dc, *Daucus carota* (AB360853).

These data accordingly recapitulate the miR168-driven cleavage of Arabidopsis *AGO1* mRNA (Rhoades et al., 2002; Vaucheret et al., 2004).

Taking advantage of the presence of a polymorphic nucleotide at position 380 (Fig. 2B, base N), which is located eight nucleotides downstream of the miR168 target sequence, we could discriminate the miR168-driven cleavage events for *NbAGO1-1L* and *NbAGO1-1H* (i.e. C and A, respectively, in Fig. 2A). Thus, the 5′ RACE revealed a proportion of one H species (characterized by the A nucleotide) versus nine L species (characterized by the C nucleotide; Fig. 2B). These data suggest that both *NbAGO1-1* transcripts were targeted and cleaved by the miRNA-mediated silencing machinery; however, the cleavage remnants that were identified by the 5′-RACE analysis (see above) more frequently derived from the L homeolog.

The 18-Nucleotide-Long Indel Affects the miR168-Mediated Expression of a GFP Reporter Gene

It was previously shown in vivo as well as in vitro that the accessibility of small RNA target sites directly correlates with target recognition and with the efficiency of cleavage, thus indicating that RISC is unable to unfold structured RNA of both endogenous or exogenous origin (i.e. mRNAs or viral RNAs, respectively; Ameres et al., 2007; Long et al., 2007; Schuck et al., 2013). This has been shown most convincingly in animal systems, but it is widely accepted also in plant systems for antiviral RISC that likely involve components similar to those involved in miRNA-mediated RNA silencing (e.g. AGO1; for review, see Ding and Voinnet, 2007). The 18-nucleotide-long indel is GC rich (12 nucleotides out of 18; it contains eight Cs, four Gs, and six Us), and its close proximity to the miR168 target region (Fig. 2A) prompted us to examine the secondary structure of the region in the *NbAGO1-1H* and *NbAGO1-1L* context. Therefore, we submitted two stretches of sequence from positions 265 to 378 (for *NbAGO1-1L*) and from positions 265 to 396 (for *NbAGO1-1H*) to Mfold (Zuker, 2003; Supplemental Fig. S1, coding sequence section). The output of the program is shown in Figure 3A. It suggested that the *NbAGO1-1H (265-396)* RNA is stably structured in this region and that the miR168 target sequence is masked

by endogenous base pairings (Fig. 3A, left). In contrast, in the *NbAGO1-1L (265-378)* RNA, the miR168-binding site was suggested to be less structured; accordingly, it seems more accessible to miRNA-directed targeting (Fig. 3A, left versus right).

To experimentally verify the predicted Mfold structures, we performed chemical modification experiments. Thus, transcripts *NbAGO1-1L (265-378)* and *NbAGO1-1H (265-396)* were generated by T7 polymerase-driven in vitro transcription from appropriate PCR amplicons and treated with dimethyl sulfate (DMS; see "Materials and Methods"). DMS specifically modifies (methylates) unpaired A and C nucleotides. The sites of chemical modification were subsequently determined by primer extension (see "Materials and Methods"); the identification of the modified nucleotides was enabled by a side-by-side electrophoresis of a DNA sequencing reaction. Figure 3B shows the experiment-deduced RNA structure, where the DMS-modified As and Cs are highlighted by green asterisks. In sum, the experimental data were in robust agreement with the obtained Mfold predictions (compare nucleotides marked by green asterisks in Fig. 3, A and B). Most interestingly, the structures of both transcripts differed considerably. That is, the transcript *NbAGO1-1L (265-378)* turned out to be significantly more accessible to chemical modifications, particularly the region that represents the target site of the miR168 seed sequence (Figs. 2B and 3B; see "Discussion").

Next, we asked if the 18-nucleotide indel and its predicted impact on the mRNA's secondary structures affected miR168-directed PTGS. For this purpose, we adopted a strategy that was earlier applied to monitor the miR171 cleavage of target RNA in planta (Parizotto et al., 2004; Lakatos et al., 2006). Binary vectors were generated that enabled *Agrobacterium tumefaciens*-mediated transient expression of two alternative reporter mRNAs via the 35S promoter in *N. benthamiana* (Fig. 3C). Each of these mRNAs consisted of the open reading frame encoding the GFP sensor and a flanking 3′ untranslated region, which contained either the H or the L sequence elements (Fig. 3A). The reporter sequences were transiently coexpressed with the viral suppressor P19 in order to prevent any transgene silencing and to isolate the effect of the plant RISC loaded with the endogenous miRNAs (Lakatos et al., 2006). Visual inspection by UV light revealed that the expressed GFP from GFP *NbAGO1-1L (256-378)* was barely detectable at 3 d post agroinfiltration (dpa). In contrast, expression of the reporter was high in leaves that were infiltrated with GFP *NbAGO1-1H (256-396)* and with the negative control (no target (Fig. 3C). This trend was confirmed when we quantified the amounts of the GFP sensor mRNAs at 1, 2, and 3 dpa by quantitative reverse transcription (qRT)-PCR (Fig. 3D). In sum, both sets of data revealed that, in the agroinfiltrated leaves at the indicated time points, the GFP *NbAGO1-1L (256-378)* mRNA showed a lower level of expression than the GFP *NbAGO1-1H (256-396)* version (Fig. 3, C and D). Importantly, when we performed a 3′-RACE analysis of the GFP reporter RNAs that were extracted from the agroinfiltrated spots, we obtained two colonies for GFP *NbAGO1-1L (256-378)* and 17 colonies for GFP *NbAGO1-1H (256-396)*. All the sequences revealed miR168-directed cleavage, which was congruent to the data that were obtained earlier with the *NbAGO1-1L* and *NbAGO1-1H* transcripts in planta (Figs. 2B and 3C). These observations provided further direct evidence that the strong down-regulation of the reporter expression, which carried the miR168 target region in the *NbAGO1-1L* context, was caused by an efficient miR168-driven cleavage.

NbAGO1-1L Is Underrepresented in the Course of a CymRSV Infection

Plant virus infections correlate with a significant accumulation of miR168 in infected tissues (Zhang et al., 2006; Csorba et al., 2007; Havelda et al., 2008; Várallyay et al., 2010, 2014; Lang et al., 2011). The reasons leading to this phenomenon are yet uncertain. They may be attributed either to a direct induction of miR168 expression (e.g. by viral components such as viral suppressors; Várallyay and Havelda, 2013) or to an induction of *AGO1* mRNA expression, which, in turn, may lead to a stabilization of miR168 via incorporation into the AGO1 protein (Vaucheret et al., 2006).

To gain further insights into the miR168-mediated posttranscriptional control of *NbAGO1-1* mRNAs, we used the well-characterized CymRSV/*N. benthamiana* system. Taking advantage of the 18-nucleotide-long indel as the main sequence difference between the two homeolog mRNAs, specific oligonucleotides were designed to enable a fine discrimination between the *NbAGO1-1L* and *NbAGO1-1H* transcripts (procedure reported in Supplemental Fig. S5). Measuring the levels of the *NbAGO1-1* mRNAs by qRT-PCR, we observed that in the course of a CymRSV infection, the amounts of *NbAGO1-1* mRNAs increased dramatically up to 4 d post inoculation (dpi; Fig. 4A), which is in line with earlier observations by Várallyay et al. (2010). However, when discriminating *NbAGO1-1L* from *NbAGO1-1H*, the scenario revealed other valuable details (Fig. 4A). Initially, in mock-inoculated plants, the ratio between *NbAGO1-1L* and *NbAGO1-1H* mRNAs was about 2:1. Conversely, at 3 dpi, the L:H ratio was inverted to 1:4. As explained, the levels of both H and L mRNAs continued to rise up to 4 dpi, although the ratio remained unaltered. At 6 dpi, the *NbAGO1-1L* transcripts reached a level close to 0, while the level of the *NbAGO1-1H* transcripts still was 8 times higher than in the mock-inoculated plants. At 10 dpi, the levels of both transcripts approximated 0, most likely because all tissues of the infected plants were already necrotic. Thus, during a viral infection that induces the accumulation of *NbAGO1-1* mRNAs and that is also accompanied by miR168 up-regulation (Vaucheret et al., 2004), the amount of the *NbAGO1-1H* variant was found to be particularly increased (Fig. 4). These data are in close agreement with the earlier observed

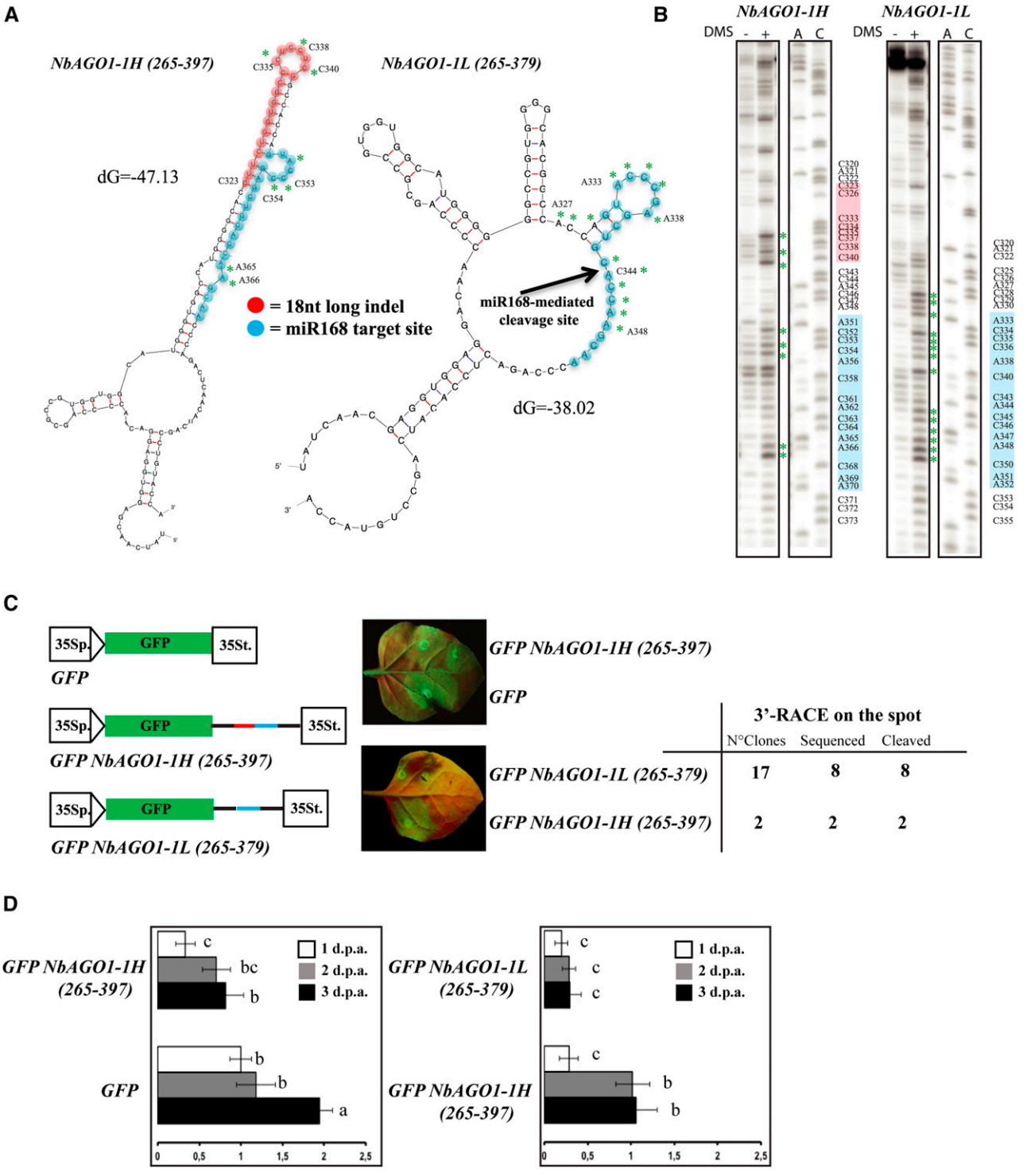

Figure 3. miR168-resistent target site in *NbAGO1-1*. A, Mfold output showing the secondary structures of *NbAGO1-1H* (left) and *NbAGO1-1L* (right) in the region containing the miR168 target site. B, Chemical probing (DMS) of RNA secondary structure and primer extension analysis. Green asterisks in A and B indicate modified bases. C, In vivo analysis of GFP *NbAGO1-1* sensor sequences. Spots in leaf halves were infiltrated with *A. tumefaciens* containing the indicated sensor sequences. The miR168 target site sequence is shown in red; the differential 18-nucleotide-long indel is shown in blue. At right is a table showing the 3′-RACE analysis on the spot. D, Relative expression levels of *GFP* mRNA in the analysis of GFP *NbAGO1-1* sensor sequences. Data are presented as means ± SE of three replicates; different letters denote significant differences at $P \leq 0.05$. GFP mRNA at 1 dpa = 1.

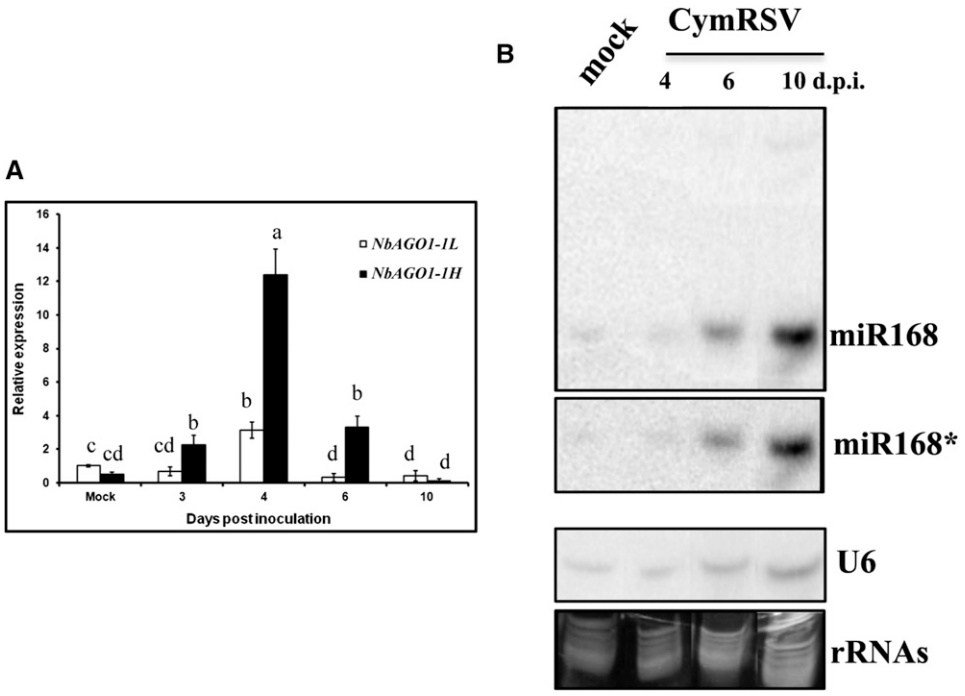

Figure 4. Relative expression of *NbAGO1-1L* and *NbAGO1-1H* during CymRSV infection. A, qRT-PCR of the two alternative transcripts; amplification was normalized to *CPH* transcripts. Data are presented as means ± SE of three replicates; different letters denote significant differences at $P \leq 0.05$. B, Northern-blot analysis of miR168 and miR168* during CymRSV infection. rRNA, Ribosomal RNA.

frequencies of transcripts and miR168-mediated cleavage products (see above).

Both NbAGO1 Homeologs Are Catalytically Active

Based on the transcript sequences, putative AGO1 H and L proteins were deduced and aligned using ClustalW (Thompson et al., 1994). A subsequent phylogenetic inspection of Arabidopsis AGO proteins using MultiAlin (http://multalin.toulouse.inra.fr/multalin/) confirmed that the two putative proteins are strongly related and that each belongs to the Arabidopsis AGO1 clade (Vaucheret, 2008; Fig. 5A): in the scheme shown in Figure 5B, amino acid substitutions are highlighted as black boxes while the indel is indicated by the white box. Considering that differences in the N-terminal sequence of human AGO1 were earlier indicated to tune the catalytic activity of the protein (Hauptmann et al., 2013), this prompted us to determine whether the two AGO homeologs are functional (i.e. whether they display a comparable AGO/RISC-mediated RNA cleavage [slicer] activity). However, the evaluation of the biological relevance of the two AGO1 homeologs in planta is difficult, mostly because a differential functional characterization of the H and L AGO1 proteins is impeded by their close similarity (Fig. 5B). For these reasons, we decided to perform this set of experiments in an in vitro system. This system, which is based on cytoplasmic extracts of *Nicotiana tabacum* BY-2 cells (BY-2 cell lysate [BYL]), is capable of reconstituting active RISC with in vitro-translated Arabidopsis, *N. benthamiana*, or *N. tabacum* AGO1 proteins and effectively recapitulates small RNA-driven mRNA regulation (Iki et al., 2010) as well as vsiRNA-driven antiviral silencing (Schuck et al., 2013). In the experiments performed, *NbAGO1-1H* and *NbAGO1-1L* cDNAs were in vitro transcribed and the corresponding proteins produced by in vitro translation in the BYL. Importantly, the translation reaction was carried out in the absence and presence of two types of siRNAs, siRNA gf698 and vsiRNA1. These siRNAs were earlier demonstrated to program reconstituted AGO1/RISC such that a GFP-encoding target mRNA and a viral RNA (a TBSV defective interfering RNA) are efficiently targeted and cleaved, respectively (Iki et al., 2010; Schuck et al., 2013). As shown in Figure 6, both types of RISC reconstituted with either the NbAGO1-1H or NbAGO1-1L protein efficiently cleaved their respective target RNA dependent on the programming siRNA. Thus, in comparison with the control reaction, 5′ and 3′ cleavage products were clearly detectable (Fig. 6). Accordingly, we concluded that both NbAGO1-1 homeologs effectively incorporated siRNAs and formed a RISC that was able to slice mRNA and viral RNA targets, respectively.

VIGS of *NbAGO1-1H*, Viral Accumulation, and Silencing of Endogenous Genes

The genetic dissection of homeolog genes that differ only in a few stretches of sequences in *N. benthamiana* is not an easy task, and it is further complicated by the fact that AGO1 is essentially involved in basic functions of plant development (Vaucheret, 2008). However, it is possible to silence Argonaute genes in *N. benthamiana* by VIGS via a tobacco rattle virus vector (Jones et al., 2006). Considering a similar approach, we

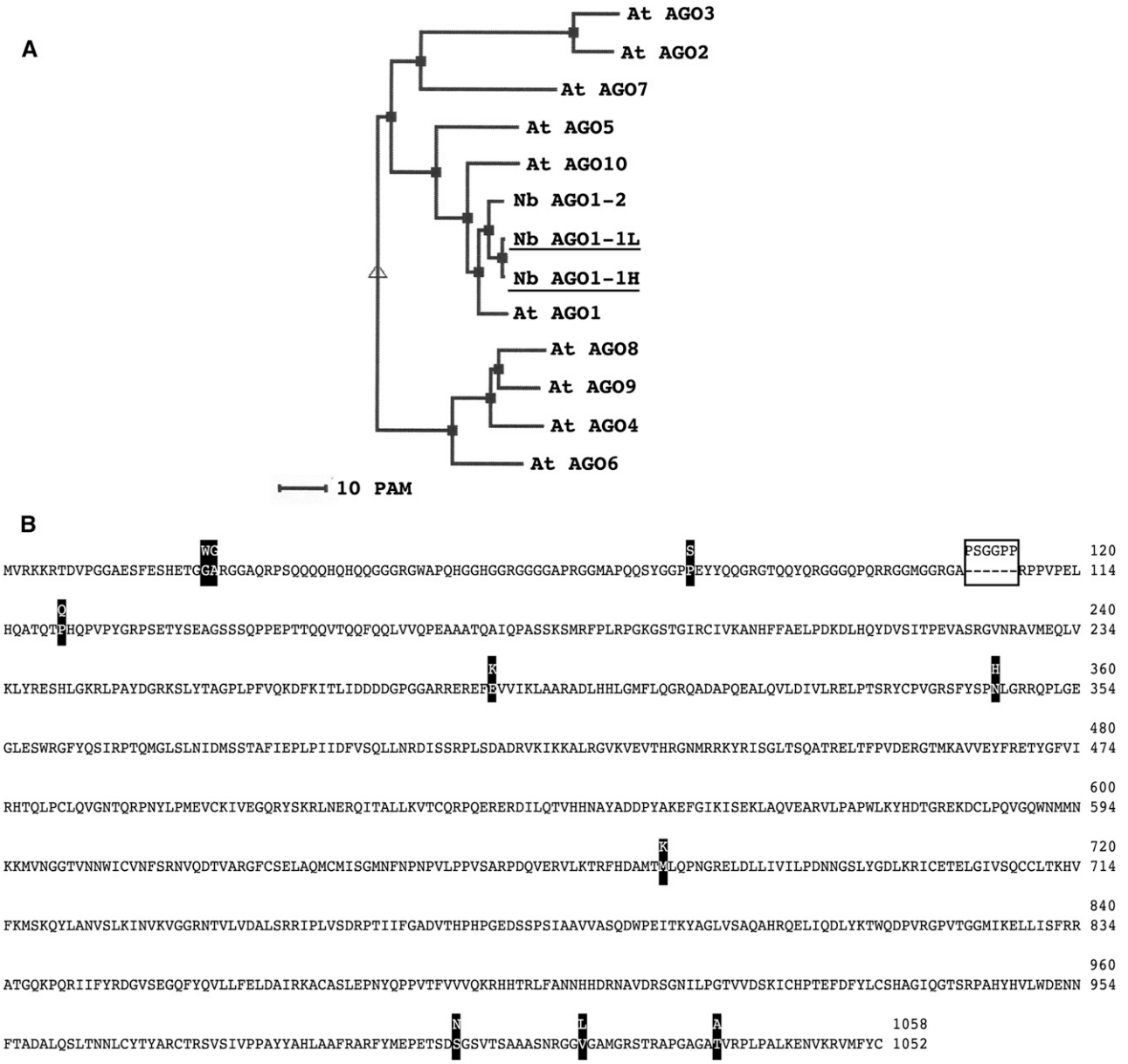

Figure 5. NbAGO1-1 proteins. A, Phylogenetic classification of *N. benthamiana* AGO1 and the Arabidopsis AGO proteins depicted in three clades. PAM indicates the point-accepted mutation. B, NbAGO1-1 predicted protein sequence showing amino acid differences between the H and L forms.

took advantage of the study of Pignatta et al. (2007), who developed a TBSV-based vector. Thus, as a first approach, we inoculated *N. benthamiana* plants with in vitro transcripts of an empty TBSV (control) and a TBSV:*NbAGO1-1* vector (Fig. 7A; for details, see "Materials and Methods"). Both sets of infected plants started to show typical symptoms of a tombusvirus infection, including necrosis in inoculated and systemic leaves at 3 to 4 dpi. However, in contrast to the control plants, the plants that were infected by TBSV:*NbAGO1-1* rapidly showed necrotic symptoms leading to a quick decline until death at 10 dpi (Fig. 7A). The increased sensitivity of the plant to viral infection as a consequence of the silencing of *NbAGO1-1* is in line with a previous report (Jones et al., 2006) and emphasizes the central role of AGO1 in RNA silencing-based antiviral defense (for review, see Burgyán and Havelda, 2011).

The fragment that was used in the TBSV:*NbAGO1-1* construct is homologous to both *NbAGO1-1H* and *NbAGO1-1L* sequences; accordingly, it induced silencing of both transcripts (see "Materials and Methods"; Supplemental Fig. S1). In order to specifically dissect the relevance of the two homeologs, we next developed a TBSV vector that carried the sequence of the indel H

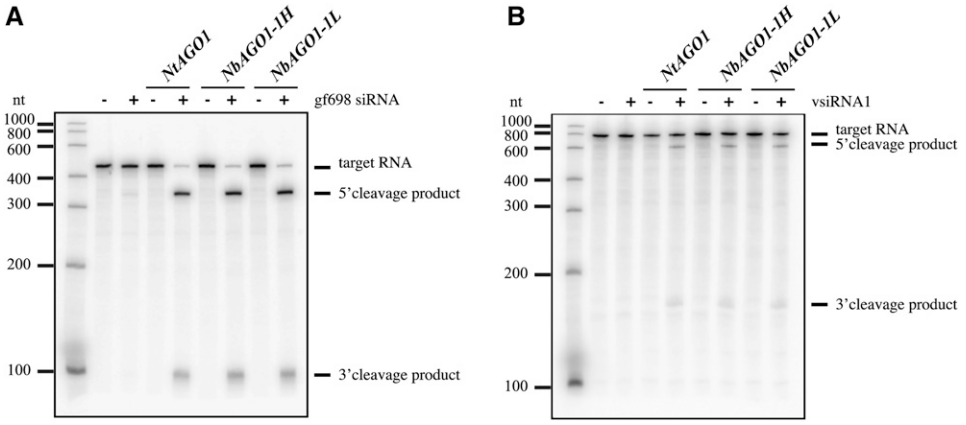

Figure 6. In vitro slicer activity of NbAGO1-1H and NbAGO1-1L. A, *NbAGO1-1* mRNAs were translated in *N. tabacum* BYL in the absence or presence of an exogenous siRNA (gf698) targeting the mRNA of GFP (Iki et al., 2010). Subsequently, a ^{32}P-labeled GFP mRNA fragment was added as a target, and RISC cleavage products were analyzed by denaturing PAGE and autoradiography. As negative and positive controls, the reactions were carried out in the absence of additionally expressed (in vitro-translated) NbAGO1 and with NtAGO1, respectively. B, The assay was performed as described above except that a TBSV defective interfering RNA was targeted by a vsiRNA, vsiRNA1 (Schuck et al., 2013).

that should consequently silence solely *NbAGO1-1H*. As explained, *NbAGO1-1H* transcripts accumulate at higher levels in virus-infected plant tissues (Fig. 4A). Hence, the TBSV-mediated VIGS was expected to reveal the specific function of NbAGO1-1H in antiviral activity and/or symptom development during a viral infection. In the subsequently performed experiment, we applied a construct that carried an additional flanking sequence that was believed to also silence the *N. benthamiana* endogenous phytoene desaturase (*PDS*; TBSV:*indelH/PDS* in Fig. 7B, top). PDS is an enzyme that is involved in intermediate steps in carotene biosynthesis. Accordingly, virus-induced silencing of this gene was expected to result in decoloration of infected tissues, which, in turn, should enable us to visually follow the silencing capacity of the viral vector (Pignatta et al., 2007). As a positive control, a TBSV construct was used that silenced solely the *PDS*. Thus, *N. benthamiana* plants were inoculated with TBSV:*PDS* and TBSV:*indelH/PDS* in vitro transcripts, and the accumulation of viral RNA was monitored on systemic leaves. As shown in Figure 7B, viral genomic RNA was detectable; it reached a peak at 6 dpi and was comparable in both cases (Figure 7B, bottom, lanes 2 and 3). Semiquantitative reverse transcription (RT)-PCR on total RNA that was extracted from six apical leaves at the recovery stage further supported that the levels of TBSV:*PDS* and TBSV:*indelH/PDS* accumulation were comparable, since the amplification product appeared at the 21st cycle with both infective constructs (Fig. 7C). Note that the amplified product of the semiquantitative RT-PCR contained the indel H fragment, which, accordingly, was verified to be retained by the TBSV vector during plant infection and spread (Fig. 7C, double asterisks; Sanger sequence not shown). These results revealed that the two vectors could accumulate at comparable levels in systemic leaves; the indel H insert was ensured to neither alter the capability of the viral vector to move long distances nor to replicate and to accumulate in infected tissues.

When we estimated the levels of *PDS* transcripts in TBSV:*PDS*- and TBSV:*indelH/PDS*-infected plants, as expected, both constructs were found to reduce the *PDS* mRNA to a level that was at least 1,000 times lower than in mock-inoculated plants. That is, in mock-inoculated plants, a discrete amplified product appeared at cycle 15 in the semiquantitative RT-PCR, while it appeared at cycle 28 in plants that had been infected with each of the TBSV constructs (Fig. 7C). Unexpectedly, though, in the recovered leaves, the whitening symptoms, which were attributed to *PDS* silencing, turned out to be visually different when we compared the plants that were infected with the two constructs. Indeed, in the case of TBSV:*indelH/PDS*, the whitening appeared brighter and more widely distributed among all newly recovered leaves, and this phenotype was found in all biological tests (Fig. 7, D and E). Conversely, with TBSV:*PDS*, the whitening appeared noticeably more confined to the leaf veins, as shown in the top right images in Figure 7, D and E. When we measured the level of the *NbAGO1-1L* and *NbAGO1-1H* transcripts, TBSV:*indelH/PDS* was confirmed to be effective in the silencing of *NbAGO1-1H*. This became most obvious at 6 dpi, when the transcript was almost undetectable (Fig. 7F). In contrast, in the case of the TBSV:*PDS*-infected tissues, the *NbAGO1-1H* transcript accumulated at a higher level than the *NbAGO1-1L* mRNA (Fig. 7F), which recapitulated the situation of the CymRSV infection shown in Figure 2C. Therefore, we concluded that the *NbAGO1-1H* homeolog, besides acting as an antiviral component, also has a

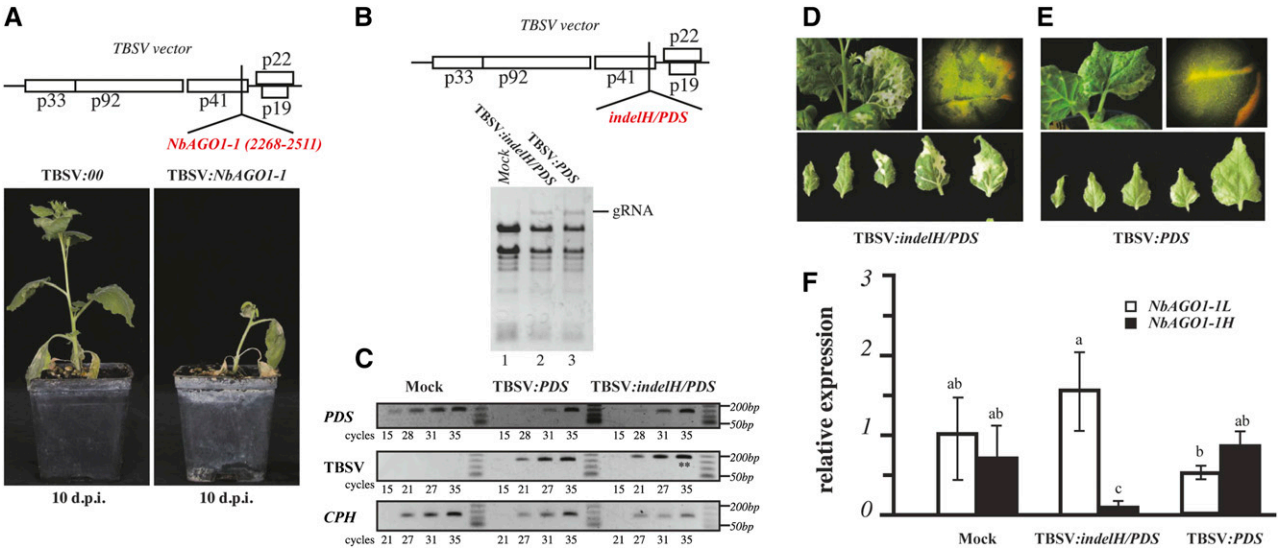

Figure 7. VIGS of *NbAGO1-1H*. A, Schematic representation of the TBSV viral vector containing a fragment inducing the silencing of *NbAGO1-1* transcripts and the effect of viral vectors on *N. benthamiana* plants at 10 dpi. B, Schematic representation of the TBSV viral vector containing the fragment that induces the silencing of *NbAGO1-1H* and *PDS* transcripts. The analysis of viral genomic RNA accumulation is shown in total RNA from infected tissues at 6 dpi. C, Semiquantitative RT-PCR analysis of the viral RNA (TBSV row), the *PDS* transcripts (PDS row), and the endogenous control gene CYCLOPHYLIN (CPH; CPH row). Double asterisks highlight the amplified products containing the indel. D and E, Visual inspection of the leaf whitening associated with *PDS* silencing in TBSV:*indelH/PDS*- and TBSV:*PDS*-infected plants, respectively. F, qRT-PCR of *NbAGO1-1H* and *NbAGO1-1L* transcripts in mock-inoculated and TBSV:*indelH/PDS*- and TBSV:*PDS*-infected plants. Data are presented as means ± SE of three replicates; different letters denote significant differences at $P \leq 0.05$.

significant impact on plant symptom development (see below).

DISCUSSION

NbAGO1-1H and *NbAGO1-1L* Loci and Transcripts

Like the majority of flowering plants, *N. benthamiana* (n = 19) possesses an allopolyploid genome (Goodin et al., 2008), as it underwent a process of whole-genome duplication through the recombination of two or more genomes from yet unidentified *Nicotiana* spp. progenitors (alloploidization). In this study, we show that *N. benthamiana* possesses two *NbAGO1-1* loci. Likely, the *NbAGO1-1L* and *NbAGO1-1H* loci derived from such genome duplications; therefore, they can be considered as *AGO1* homeologs. Genome duplication, except in cases of redundancy, is often followed by changes in gene expression/gene specialization (subfunctionalization), evolution of a novel function (neofunctionalization), or gene loss (nonfunctionalization including the generation of pseudogenes; Comai et al., 2000). For example, a phylogenetic approach carried out on *N. tabacum* (a close relative of *N. benthamiana*) and its progenitors *Nicotiana tomentosiformis* and *Nicotiana sylvestris* showed that about 90% of all homeolog sequences (6% of all genes) maintained the expression of only one homeolog, since the second homeolog was lost after genome duplication and evolution (Bombarely et al., 2012a).

Instead, in the *N. benthamiana* allopolyploid context, we show that both *NbAGO1-1L* and *NbAGO1-1H* homeologs retained the full capacity to transcribe mRNAs. Strikingly, a previous study (Nakasugi et al., 2013), which aimed to identify all the *N. benthamiana* RNA-silencing genes, did not highlight the presence of the *NbAGO1-1L* transcript. The authors describe two *AGO1* transcripts, named *AGO1a* and *AGO1b*, both containing the indel. That the *NbAGO1-1L* transcript was missed is probably due to the fact that the *NbAGO1* transcript that lacks the 18-nucleotide-long indel was poorly represented in the unigene data set (i.e. one out of eight *AGO1.1* species; see above and Supplemental Fig. S3). Another explanation may be that the 18-nucleotide-long insertion in the *AGO1* transcript is conserved among the Solanaceae (Fig. 2A, top) and, accordingly, was used as a reference sequence in the RNA sequencing assembly processes.

Our findings indicate that an 18-nucleotide-long GC-rich element in the *NbAGO1-1* mRNA has important functional implications for the modulation of AGO1 expression in *N. benthamiana*. Interestingly, the element is missing in only one type of the known *NbAGO1-1* mRNAs (Fig. 2A), and it has no evident consequences, either on the expression or on the functionality of the proteins, at least in the in vitro functional analysis performed here (Fig. 6; see below). Hence, it may be hypothesized that the speciation of *N. benthamiana* following allopolyploidization has resulted in two alternative transcripts of *AGO1-1*, the expression of which is

differently regulated by miRNA-mediated cleavage at the posttranscriptional level. One interpretation of our findings involves the possibility that the *NbAGO1-1H* locus developed from the *NbAGO1-1L* locus and that this led to the expression of an mRNA that is less accessible to miR168 cleavage.

Regarding the level of expression of the two transcripts, our qRT-PCR data indicate that, in naive plants, the H form of *NbAGO1-1* is slightly less abundant than the L form (i.e. 1:2; Figs. 4A and 7F, mock-inoculated plants). This could be due to a different transcriptional control, which deserves further specific investigation. It also remains unclear whether the two transcripts coexist in the same cells and whether they are spatially and/or temporally separated from the regulatory RISC (Souret et al., 2004; Brodersen et al., 2008).

The Indel and the miR168-Mediated Regulation of Transcripts

In a previous study on the activity of human RISC, Ameres et al. (2007) revealed that the accessibility of the target site directly correlates with the efficiency of the cleavage reaction. The two *NbAGO1-1* homeolog transcripts differ in the 18-nucleotide-long indel, which is located only eight nucleotides upstream of the miR168 target site (Fig. 1C), and our prediction as well as experimental data suggest that this has considerable consequences for the formation of the secondary RNA structure of the miR168 target site. The presence of the indel in *NbAGO1-1H* appears to mask the miR168 target site and, thus, may render miR168 posttranscriptional regulation more difficult. This is in contrast with the situation with *NbAGO1-1L*, which was indicated to be clearly more accessible to the miR168 seed sequence (Fig. 3, A and B). This notion was further supported when we transferred the same sequence stretch into the context of the GFP reporter construct. The 18-nucleotide-long insertion had an evident effect on protein expression and mRNA accumulation, likely through a different sensitivity to miR168-mediated PTGS (Fig. 3, C and D). The idea that miR168-mediated cleavage of *NbAGO1-1H* occurs less efficiently (or less frequently) than *NbAGO1-1L* cleavage is also fueled by the 3′- and 5′-RACE data that were obtained in the GFP reporter gene context and during the in vivo analysis (Figs. 2B and 3C). Our analyses were performed with only one stretch of the *NbAGO1-1H* or *NbAGO1-1L* transcript, and we are aware that the results may not necessarily reproduce the same functionality in the whole RNA context. Unfortunately, a further detailed analysis in planta is impeded by the close similarity of the two homeologs. However, the sum of in silico, in vitro, and in vivo data supports our model, proposing that the 18-nucleotide-long indel represents an important modulator of the RNA structure that involves also the miR168 target site, which, when it is present, may confer a lower sensitivity, and upon its loss, may confer a higher sensitivity, to miR168-guided cleavage.

These data prompted us to look at transcript data that are available for other Solanaceae spp. and to search for variants that may have a similar impact on the miR168 target sites. Interestingly, the *Solanum lycopersicum AGO1A*-like and *AGO1B* (and *Solanum tuberosum AGO1*-like and *AGO1B*-like) alignment reveals one 21-nucleotide-long indel that is located 22 nucleotides downstream of the miR168 target site (Supplemental Fig. S6). In silico folding of these regions suggests that this indel may affect the secondary structure and accessibility of the miR168 target site of the *Solanum* spp. *AGO1* mRNA in a similar way to that found here with *NbAGO1-1H* and *NbAGO1-1L* of *N. benthamiana* (data not shown).

Moreover, a recent *S. lycopersicum* genome-wide analysis of 5′-uncapped mRNAs (i.e. products of miRNA cleavages; German et al., 2008) suggests that both *S. lycopersicum* AGO1A-like and AGO1B are controlled by miR168 (Lopez-Gomollon et al., 2012). This is an additional indication that the presence of indels around the miR168 target site does not abolish cleavage-based posttranscriptional regulation events. Instead, these elements appear to play a role in the fine-tuning of the expression of duplicate genes and homeologs during conditions of miR168 up-regulation, such as under stress induced by viral infections.

NbAGO1-1 Homeologs in Viral Infection

N. benthamiana is widely considered as a model host for virus-plant interaction studies, and it has also been successfully used in molecular studies of RNA silencing-based plant-virus interactions with tombusvirus systems. Here, we applied CymRSV because the functionality of miR168 in *N. benthamiana* during a CymRSV infection was convincingly demonstrated by Várallyay et al. (2014). Indeed, we considered this virus system most adequate to dissect the miR168-directed regulation of the *NbAGO1-1* mRNAs for the following reasons: (1) *N. benthamiana* plants show a strong accumulation of miR168 associated with a CymRSV infection (Fig. 4B; Várallyay et al., 2010); (2) while not binding miR168 (Várallyay et al., 2014), the viral suppressor P19 is supposed to effectively sequester vsiRNAs and to impede their interference with endogenous and physiological AGO1 functionalities (at least during the initial stages of infection and spread); and (3) the level of *NbAGO1-1* mRNA seems to increase in CymRSV-infected plants, but this is not associated with an accumulation of mRNA cleavage products (Várallyay et al., 2010). Earlier works detected miRNA-mediated *NbAGO1* mRNA cleavage in virus-infected cells at a lower extent than in naive cells (Várallyay et al., 2010), and our findings are consistent with these data, if we consider solely the situation with *NbAGO1-1H* (Fig. 2C). Várallyay et al. (2010) also observed a reduction of AGO1 protein accumulation and attributed this contradiction (i.e. up-regulation of AGO1 mRNA and miR168 but no increase of 5′ cleavage products) to an miRNA-mediated translation inhibition of the

mRNA. Obviously, the above studies and conclusions did not discriminate between the two homeolog transcripts and were based on measurements of the total amount of both *NbAGO1-1* mRNAs. As explained above, the two *NbAGO1-1* homeologs were targeted and cleaved by miR168; however, the cleavage remnants of the H homeolog were less detectable by RACE analysis. Thus, it is conceivable that the measured cleavage products mainly derived from the L version of the *NbAGO1* mRNA, while the H version, which is cleaved to a considerably lower extent, indeed is translationally repressed, as suggested by Várallyay et al. (2010). Future experiments need to address this interesting aspect.

A VIGS strategy was used as a preliminary approach to dissect the functionality of the two *NbAGO1-1* homeologs. This strategy was based on the widely accepted assumption that AGO1 represents a major effector of PTGS of endogenous genes (Bologna and Voinnet, 2014). Thus, plants that were infected with TBSV:*NbAGO1-1*, which silenced both *NbAGO1-1* homeologs, underwent a quick necrotic decline (Fig. 7A). Considering that both NbAGO1-1H and NbAGO1-1L are able to incorporate siRNAs and to reconstitute RISC active in cleaving viral RNA in vitro (Fig. 6), these data suggest that both homeolog genes together constitute a solid layer of defense against tombusvirus infections. In other words, both homeologs were indicated to be determinants of the susceptibility of *N. benthamiana* to infections with tombusviruses.

The application of a construct that was able to silence the endogenous *PDS* gene and specifically *NbAGO1-1H* highlighted another intriguing aspect. While at 6 dpi, we could achieve an efficient silencing of *NbAGO1-1H* (Fig. 7F), no differences in viral accumulation or necrosis were observed in comparison with the control (Fig. 7, B–E). However, as explained in "Results," the whitening symptoms, which were associated with the silencing of the endogenous *PDS* gene, revealed evident differences between plants that were treated with TBSV:*indelH/PDS* and the TBSV:*PDS* control plants (Fig. 7, D and E). Closely consistent with our earlier data, we found the *NbAGO1-1L* transcript to be expressed almost twice as much as *NbAGO1-1H* in the mock-inoculated plants (Figs. 4A and 7F). During the infection, this ratio turned around (i.e. the amount of the *NbAGO1-1L* transcript decreased and the amount of *NbAGO1-1H* increased), which was explained again by the increase of miR168 expression and the lower sensitivity of *NbAGO1-1H* to miR168 cleavage. When forcing the silencing of *NbAGO1-1H* using VIGS, the plants showed again an increasing amount of the L form (Fig. 7F). This may suggest that the loss of the H form is somehow compensated by a higher gene expression of the L form to control the invasion of the virus.

The current status of our findings clearly supports the view that the presence of two forms of AGO1-1 represents an evolutionary advantage for the plant. Thus, both AGO1-1 forms were indicated to operate in concert to ensure basic mRNA regulatory control during conditions of stress, such as a viral infection where massive amounts of vsiRNAs are produced and where miR168 expression is up-regulated. Along this line, the presence of short indels in close proximity to miRNA target sites may represent a new type of genetic strategy to fine-tune the miRNA-mediated posttranscriptional regulation of genes under stress.

This speculation is, at least in part, supported by recent reports with Arabidopsis showing (1) the necessary presence of two specialized pools of AGO1 that are loaded with single classes of short RNA duplexes (i.e. with either miRNAs or viral siRNAs; Schott et al., 2012) and (2) the evidence that recovery and VIGS are mediated by different host factors, including AGO1 (Ma et al., 2015). Thus, our data add another layer of regulation of the AGO1 homeostasis in plants under external stimuli. Our findings are in line with an earlier report of Li et al. (2012), who observed that miR168 overexpression does not necessarily correlate with lower AGO1 mRNA levels.

As such, this study provides an important basis for future molecular, biochemical, and genome-wide studies aimed at unraveling the mechanisms of the functional diversification of genes involved in RNA silencing, with a particular relevance in the context of polyploidy.

MATERIALS AND METHODS

Bioinformatics Analysis

The draft genome of *Nicotiana benthamiana* (version 0.4.4) was downloaded from http://solgenomics.net/organism/Nicotiana_benthamiana/genome (Bombarely et al., 2012b). It comprises a set of 140,890 scaffolds (with a total length of 2,593,640,036 bp), which were imported into the CLC Genomics Workbench software (version 5.5) for further analysis. The scaffolds were screened for the presence of *NbAGO1* (National Center for Biotechnology Information accession number DQ321488; 3,156 bp). Sequence matches were found on two distinct scaffolds, SCF00034990 and SCF00010009. From a pairwise alignment between the two alternative *NbAGO1* gene sequences, point mutations (single-nucleotide and deletion-insertion polymorphisms) were detected as well as an 18-bp deletion (on scaffold SCF00034990). We defined the transcript containing the full gene sequence as *NbAGO1-1H*; the variant containing the 18-bp deletion was termed *NbAGO1-1L*. The intron/exon structure was determined through analysis with GENSCAN (http://genes.mit.edu/GENSCANinfo.html; Burge and Karlin, 1997) accompanied by manual interpretation.

To retrieve all the annotated and putative *AGO1*-like gene sequences available in databases, the NbAGO1-1H protein sequence was submitted to tBLASTn using the plant taxid database. Annotated or predicted *AGO1*-like mRNAs containing putative miR168 target sequences were selected and multialigned with ClustalW (Thompson et al., 1994; DNA weight matrix = default value, gap open = 100, and gap extension = 10).

cDNA of *NbAGO1-1* Transcripts, GFP Sensor, and Agroinfiltration

Total RNA was extracted from 100 mg of expanded leaf tissues from *N. benthamiana* plants using TriReagent (Sigma) following the manual's instructions. Upon DNaseI (Ambion) treatment to ensure the elimination of traces of DNA, the polyadenylated fraction was enriched using the Ambion Poly(A)Purist Kit (Life Technologies). The polyadenylated fraction was used for randomized cDNA generation. Oligonucleotides NbAGOmiRNAS and NbAGOmiRNAAS (Várallyay et al., 2010) were used for PCR amplification of the approximately 120-bp-long fragment containing the miR168 target site. Two PCR species (data not shown), almost indistinguishable in size, were observed on agarose gels. Therefore, the PCR was first loaded and separated through a 2% (w/v) agarose gel and excised from the very top and very bottom of the doublet. Then, the two amplified species were again separated via an 8% (w/v) polyacrylamide gel.

From the latter gel, the species were cloned into the pGEM T-easy vector (Promega) and sequenced.

PCR product species of target sequences H and L were placed into the *Sma*I-linearized plasmid pAJ as described previously (Pantaleo et al., 2007). Sanger sequencing was used to verify the orientation of the cloned fragments. Sensor constructs pAJ GFP *NbAGO1-1L (256-379)* and pAJ-GFP *NbAGO1-1H (256-397)* were transferred into the *Agrobacterium tumefaciens* strain C58C1 as described previously (Pantaleo and Burgyán, 2008) and then agroinfiltrated into well-expanded 6- to 10-leaf-old *N. benthamiana*. After 3 dpi, the leaves were analyzed under the UV lamp.

5′- and 3′-RACE

5′-RACE analysis of miR168-cleaved *NbAGO1-1* was performed as described previously (Shimura et al., 2011) with the polyadenylated fraction obtained from total RNA of *N. benthamiana*. Polyadenylated RNA was obtained with the Ambion Poly(A)Purist Kit (Life Technologies) following the manual's instructions. A gene-specific reverse oligonucleotide for PCR having the sequence 5′-CTTCCATATGGTACAGGCTGA-3′ was designed downstream of the expected miR168 cleavage site.

3′-RACE of the GFP sensor sequence GFP-*NbAGO1-1* was carried out on the RNA extracted from the agroinfiltrated spots as described previously (Pantaleo et al., 2007). After RACE PCR amplification, the gel slice corresponding to 150 to 200 nucleotides in size was excised, and the DNA was eluted, cloned, and Sanger sequenced.

CymRSV Infection and *NbAGO1-1* mRNA qRT-PCR

The plasmid encoding the CymRSV RNA (Burgyan et al., 1990) was linearized with *Sma*I, ethanol precipitated, and transcribed in vitro using T7 RNA polymerase. *N. benthamiana* plants were inoculated with the viral RNA transcript as described (Rubino et al., 1992). Total RNA was extracted from leaf tissues with TriReagent (Invitrogen) following the manufacturer's instructions. We analyzed leaves mock inoculated and at 3, 4, 6, and 10 dpi. Primers for qRT-PCR were designed taking advantage of the 18-nucleotide-long indel, in order to discriminate the homeologs *NbAGO1-1H* and *NbAGO1-1L*: *NbAGO1-1H* for, 5′-GCCATGGGGCACCTTCTG-3′; *NbAGO1-1H* rev, 5′-GAGACGAGGAACCAGCCTC-3′; *NbAGO1-1L* for, 5′-ATCAACGAGGTGGAGGACAA-3′; and *NbAGO1-1L* rev, 5′-GGTACTGGTGGCCGTGC-3′. Primers for qRT-PCR amplification of *GFP* mRNA were GFP for (5′-CGATGGCCCTGTCCTTTTAC-3′) and GFP rev (5′-GGTCTCTCTTTTCGTTGGGATCT-3′). First strand cDNA synthesis was performed using 5 μg of total RNA treated with DNase and the High Capacity cDNA Reverse Transcription Kit (Applied Biosystems). Relative expression was calculated based on the comparative cycle threshold method as described by Livak and Schmittgen (2001). The PCR mix (10 μL) contained 5 μL of PowerSYBR Green master mix (Life Technologies), 0.25 μM of each primer, and 1 μL of cDNA diluted 1:10. Cycling conditions for *NbAGO1-1H* and *NbAGO1-1L* primer pairs consisted of initial denaturation at 95°C for 10 min, followed by 40 cycles at 95°C for 15 s, and 65°C for 1 min. Cycling conditions for *GFP* amplification consisted of initial denaturation at 95°C for 10 min, followed by 40 cycles at 95°C for 15 s, and 60°C for 1 min. Specific annealing of the primers was controlled on dissociation kinetics performed at the end of each PCR run. Expression of the *CPH* gene was used as the normalization factor in all samples as reported (Havelda et al., 2008), since *CPH* concentration in *N. benthamiana* is constant during virus infection. Transcript level was expressed as the mean and SE calculated for three replicates. Data were statistically analyzed using the ANOVA *F* test ($P \leq 0.05$).

Cell Culture and Preparation of Cytoplasmic BY-2 Cell Extract

Nicotiana tabacum BY-2 cells were cultured as described (Gursinsky et al., 2009) at 23°C in Murashige and Skoog liquid medium. Evacuolated BY-2 protoplasts to prepare cytoplasmic extract (BYL) were obtained by Percoll gradient centrifugation (Komoda et al., 2007; Gursinsky et al., 2009).

In Vitro Transcription

To generate plasmids for the production of *NbAGO1-1H* and *NbAGO1-1L* mRNAs, the corresponding open reading frames were amplified by PCR and inserted between the *Xba*I and *Sma*I sites of a modified pSP64-poly(A) vector (Promega) that contained an additional *Swa*I site downstream of the polyadenylated sequence.

Transcription and further treatment of the transcript were performed using standard procedures. Transcripts encoding firefly luciferase were generated by SP6 RNA polymerase (Thermo Scientific) from the *Xho*I-linearized plasmid pSP-luc(+) (Promega). AGO mRNAs were synthesized in the presence of the monomethylated cap analog m^7GP^3G (Jena Biosciences) from the *Swa*I-linearized plasmids using SP6 RNA polymerase. To generate the GFP target RNA, a 432-bp sequence was amplified by PCR from plasmid pGFP-C1 with the T7 promoter sequence included in the forward primer. Radioactive labeling was performed using standard conditions. TBSV defective interfering RNA was synthesized by T7 RNA polymerase from an *Sma*I-linearized template DNA (Schuck et al., 2013).

siRNAs

RNA oligonucleotides were purchased from Biomers. The sequences of the gf698 siRNA duplex were 5′-UAGUUCAUCCAUGCCAUGUGUA-3′ (guide strand) and 5′-CACAUGGCAUGGAUGAACUAUA-3′ (passenger strand). The sequences of the TBSV-derived vsiRNAs were 5′-UAUCCGACCAUAGGCCCAUGU-3′ (guide strand) and 5′-AUGGGCCUAUGGUCGGAUAAG-3′ (passenger strand). To produce siRNA duplexes, the single-stranded RNAs were incubated in annealing buffer (30 mM HEPES-KOH, pH 7.4, 100 mM potassium acetate, and 2 mM magnesium acetate) for 1 min at 90°C and annealed for 60 min at 37°C. All siRNAs used were nonphosphorylated.

In Vitro Slicer Assay

To generate AGO1 variants and siRNA-programmed AGO/RISC in vitro, the AGO mRNAs were in vitro translated in 50% (v/v) BYL in the previously described conditions (Gursinsky et al., 2009). Briefly, 1.5 μg of AGO mRNA was translated in a 20-μL reaction in the presence of 50 nM synthetic siRNA for 60 min. To measure slicer activity, the same amount of siRNA was added again, and the reaction was continued for another 90 min. Two micrograms of firefly luciferase (competitor) mRNA and the ^{32}P-labeled target RNA (50 fmol) were added, and the cleavage reaction was performed for another 15 min. Total RNA was isolated from the reaction by treatment with 20 μg of Proteinase K in the presence of 0.5% (w/v) SDS for 30 min at 37°C, followed by extraction with 1 volume of chloroform and ethanol precipitation. ^{32}P-labeled products were separated on 5% (w/v) Tris-borate polyacrylamide gels containing 8 M urea and visualized by phosphor imaging.

Virus-Induced RNA Silencing

The TBSV viral vector (pPD-A4) was kindly provided by Dr. M. Turina. The vector TBSV:*NbAGO1-1* was obtained by exchanging the *PDS* fragment in pPD-A4 with an *Xho*I (Fermentas)-digested fragment obtained by PCR amplification of the *NbAGO1-1* gene (positions 2,268–2,351; Supplemental Fig. S1) using 5′-TGCTCGAGCATACCCATGTGGCCTTGTCTTCAAG-3′ and 5′-ACACTCGAGAATATCACGTTCTCTC-3′ (*Xho*I restriction sites underlined) as oligonucleotides and total DNA extracted from leaves (Rubino et al., 1992) as substrate. For TBSV:*indelH/PDS*, oligonucleotides *pdsXhoIrev* (5′-AGGACACTCGAGCAGGAGGGTTACC-3′) and *TBSVAGO11Hfor* (5′-TAGTGCTCGAG**GCACCTTCTGGTGGCCCTCCTCGGC**ACGAGCTTTCGATG-3′; forward oligonucleotides in boldface) were used to obtain the fragment of *N. benthamiana PDS* (positions 878–973 of the ref_seq DQ469932) with the flanking 25-nucleotide-long sequence of the *NbAGO1-1H* indel. All constructs were *Sma*I restricted, and infectious RNAs were generated and inoculated as described previously (Rubino et al., 1992).

Semiquantitative RT-PCR Analysis

To control equal cDNA amounts in each reaction, PCR was performed with primers corresponding to *CPH* (see above). Primer sequences were as follows: TBSV Forward, 5′-GAGGGTTACCATCTAAAAAGGCC-3′; TBSV Reverse, 5′-CTTGTTCGTATTCAGTATCC-3′; PDS Forward, 5′-GATGCWACRATGAAGGAACTAGC-3′; PDS Reverse, 5′-GCCGACARGGTTCACAACCTG-3′.

Chemical Probing of RNA Secondary Structure and Primer Extension Analysis

Evaluation of the RNA secondary structure was done using the protocol released by Yu et al. (1999) with minor modifications. The modifying agent used was DMS (Merck). DMS modification was performed with 1 μg of in

vitro-transcribed RNA and 32 mM DMS in a 200-μL reaction mixture containing 20 mM HEPES-KOH (pH 7.9), 60 mM KCl, and 12 mM $MgCl_2$ at 30°C for 5 min. The reaction was stopped by the addition of an equal volume of DMS stop buffer containing 0.6 M sodium acetate, 0.4 M β-mercaptoethanol, 0.4 M Tris-HCl (pH 7.5), and 10 mM EDTA. The modified RNA was then ethanol precipitated with 10 μg of tRNA as a carrier.

Chemically modified RNA molecules were mixed with 1 pmol of 5′ end-labeled DNA primer (5′-CGCACGCGTGGTACAGGCTGA-3′). Primer extension was performed at 42°C for 60 min with 100 units of RevertAid Reverse Transcriptase (Thermo Scientific) at standard conditions as recommended by the manufacturer. The locations of modification sites were determined by PAGE of the primer extension products (see above). In parallel, the corresponding DNA sequences were determined by dideoxynucleotide sequencing (DNA cycle sequencing kit; Jena Bioscience) with the same 5′ end-labeled primer.

Sequence data from this article can be found in the GenBank/EMBL data libraries under accession numbers KR942296 and KR942297.

Supplemental Data

The following supplemental materials are available.

Supplemental Figure S1. Sequence alignment of *NbAGO1-1L* and *NbAGO1-1H* loci.

Supplemental Figure S2. PCR-based strategy for validating *NbAGO1-1L* and *NbAGO1-1H* loci.

Supplemental Figure S3. List of *NbAGO1-1H* and *NbAGO1-1L* transcript species found in the RNA-Seq data set.

Supplemental Figure S4. Multiple alignment of miR168 family members.

Supplemental Figure S5. qRT-PCR for discriminating *NbAGO1-1H* and *NbAGO1-1L*.

Supplemental Figure S6. Multiple alignment of annotated *ARGONAUTE1* mRNAs of *Solanum lycopersicum* and *Solanum tuberosum*.

ACKNOWLEDGMENTS

We thank David S. Horner for a critical review of the article.

Received January 17, 2015; accepted May 20, 2015; published May 26, 2015.

LITERATURE CITED

Ameres SL, Martinez J, Schroeder R (2007) Molecular basis for target RNA recognition and cleavage by human RISC. Cell **130:** 101–112

Baumberger N, Baulcombe DC (2005) Arabidopsis ARGONAUTE1 is an RNA Slicer that selectively recruits microRNAs and short interfering RNAs. Proc Natl Acad Sci USA **102:** 11928–11933

Bologna NG, Voinnet O (2014) The diversity, biogenesis, and activities of endogenous silencing small RNAs in Arabidopsis. Annu Rev Plant Biol **65:** 473–503

Bombarely A, Edwards KD, Sanchez-Tamburrino J, Mueller LA (2012a) Deciphering the complex leaf transcriptome of the allotetraploid species Nicotiana tabacum: a phylogenomic perspective. BMC Genomics **13:** 406

Bombarely A, Rosli HG, Vrebalov J, Moffett P, Mueller LA, Martin GB (2012b) A draft genome sequence of Nicotiana benthamiana to enhance molecular plant-microbe biology research. Mol Plant Microbe Interact **25:** 1523–1530

Brodersen P, Sakvarelidze-Achard L, Bruun-Rasmussen M, Dunoyer P, Yamamoto YY, Sieburth L, Voinnet O (2008) Widespread translational inhibition by plant miRNAs and siRNAs. Science **320:** 1185–1190

Burge C, Karlin S (1997) Prediction of complete gene structures in human genomic DNA. J Mol Biol **268:** 78–94

Burgyán J, Havelda Z (2011) Viral suppressors of RNA silencing. Trends Plant Sci **16:** 265–272

Burgyan J, Nagy PD, Russo M (1990) Synthesis of infectious RNA from full-length cloned cDNA to RNA of cymbidium ringspot tombusvirus. J Gen Virol **71:** 1857–1860

Comai L, Tyagi AP, Winter K, Holmes-Davis R, Reynolds SH, Stevens Y, Byers B (2000) Phenotypic instability and rapid gene silencing in newly formed *Arabidopsis* allotetraploids. Plant Cell **12:** 1551–1568

Csorba T, Bovi A, Dalmay T, Burgyan J (2007) The p122 subunit of Tobacco mosaic virus replicase is a potent silencing suppressor and compromises both siRNA and miRNA mediated pathways. J Virol **81:** 11768–11780

Csorba T, Pantaleo V, Burgyán J (2009) RNA silencing: an antiviral mechanism. Adv Virus Res **75:** 35–71

Cuperus JT, Fahlgren N, Carrington JC (2011) Evolution and functional diversification of *MIRNA* genes. Plant Cell **23:** 431–442

Ding SW, Voinnet O (2007) Antiviral immunity directed by small RNAs. Cell **130:** 413–426

German MA, Pillay M, Jeong DH, Hetawal A, Luo S, Janardhanan P, Kannan V, Rymarquis LA, Nobuta K, German R, et al (2008) Global identification of microRNA-target RNA pairs by parallel analysis of RNA ends. Nat Biotechnol **26:** 941–946

Goodin MM, Zaitlin D, Naidu RA, Lommel SA (2008) Nicotiana benthamiana: its history and future as a model for plant-pathogen interactions. Mol Plant Microbe Interact **21:** 1015–1026

Gursinsky T, Schulz B, Behrens SE (2009) Replication of Tomato bushy stunt virus RNA in a plant in vitro system. Virology **390:** 250–260

Harvey JJ, Lewsey MG, Patel K, Westwood J, Heimstädt S, Carr JP, Baulcombe DC (2011) An antiviral defense role of AGO2 in plants. PLoS ONE **6:** e14639

Hauptmann J, Dueck A, Harlander S, Pfaff J, Merkl R, Meister G (2013) Turning catalytically inactive human Argonaute proteins into active slicer enzymes. Nat Struct Mol Biol **20:** 814–817

Havelda Z, Várallyay E, Válóczi A, Burgyán J (2008) Plant virus infection-induced persistent host gene downregulation in systemically infected leaves. Plant J **55:** 278–288

Iki T, Yoshikawa M, Nishikiori M, Jaudal MC, Matsumoto-Yokoyama E, Mitsuhara I, Meshi T, Ishikawa M (2010) In vitro assembly of plant RNA-induced silencing complexes facilitated by molecular chaperone HSP90. Mol Cell **39:** 282–291

Iwakawa HO, Tomari Y (2013) Molecular insights into microRNA-mediated translational repression in plants. Mol Cell **52:** 591–601

Jones L, Keining T, Eamens A, Vaistij FE (2006) Virus-induced gene silencing of *Argonaute* genes in *Nicotiana benthamiana* demonstrates that extensive systemic silencing requires *Argonaute1*-Like and *Argonaute4*-Like genes. Plant Physiol **141:** 598–606

Kidner CA, Martienssen RA (2004) Spatially restricted microRNA directs leaf polarity through ARGONAUTE1. Nature **428:** 81–84

Kidner CA, Martienssen RA (2005) The role of ARGONAUTE1 (AGO1) in meristem formation and identity. Dev Biol **280:** 504–517

Komoda K, Mawatari N, Hagiwara-Komoda Y, Naito S, Ishikawa M (2007) Identification of a ribonucleoprotein intermediate of tomato mosaic virus RNA replication complex formation. J Virol **81:** 2584–2591

Lakatos L, Csorba T, Pantaleo V, Chapman EJ, Carrington JC, Liu YP, Dolja VV, Calvino LF, López-Moya JJ, Burgyán J (2006) Small RNA binding is a common strategy to suppress RNA silencing by several viral suppressors. EMBO J **25:** 2768–2780

Lanet E, Delannoy E, Sormani R, Floris M, Brodersen P, Crété P, Voinnet O, Robaglia C (2009) Biochemical evidence for translational repression by *Arabidopsis* microRNAs. Plant Cell **21:** 1762–1768

Lang Q, Jin C, Lai L, Feng J, Chen S, Chen J (2011) Tobacco microRNAs prediction and their expression infected with Cucumber mosaic virus and Potato virus X. Mol Biol Rep **38:** 1523–1531

Li W, Cui X, Meng Z, Huang X, Xie Q, Wu H, Jin H, Zhang D, Liang W (2012) Transcriptional regulation of Arabidopsis *MIR168a* and *ARGONAUTE1* homeostasis in abscisic acid and abiotic stress responses. Plant Physiol **158:** 1279–1292

Livak KJ, Schmittgen TD (2001) Analysis of relative gene expression data using real-time quantitative PCR and the $2^{(-\Delta\Delta C(T))}$ method. Methods **25:** 402–408

Long D, Lee R, Williams P, Chan CY, Ambros V, Ding Y (2007) Potent effect of target structure on microRNA function. Nat Struct Mol Biol **14:** 287–294

Lopez-Gomollon S, Mohorianu I, Szittya G, Moulton V, Dalmay T (2012) Diverse correlation patterns between microRNAs and their targets during tomato fruit development indicates different modes of microRNA actions. Planta **236:** 1875–1887

Ma X, Nicole MC, Meteignier LV, Hong N, Wang G, Moffett P (2015) Different roles for RNA silencing and RNA processing components in virus recovery and virus-induced gene silencing in plants. J Exp Bot **66:** 919–932

Nakasugi K, Crowhurst RN, Bally J, Wood CC, Hellens RP, Waterhouse PM (2013) De novo transcriptome sequence assembly and analysis of RNA silencing genes of Nicotiana benthamiana. PLoS ONE **8:** e59534

Navarro B, Russo M, Pantaleo V, Rubino L (2006) Cytological analysis of Saccharomyces cerevisiae cells supporting cymbidium ringspot virus defective interfering RNA replication. J Gen Virol **87:** 705–714

Omarov R, Sparks K, Smith L, Zindovic J, Scholthof HB (2006) Biological relevance of a stable biochemical interaction between the tombusvirus-encoded P19 and short interfering RNAs. J Virol **80:** 3000–3008

Panavas T, Nagy PD (2003) Yeast as a model host to study replication and recombination of defective interfering RNA of Tomato bushy stunt virus. Virology **314:** 315–325

Pantaleo V, Burgyán J (2008) Cymbidium ringspot virus harnesses RNA silencing to control the accumulation of virus parasite satellite RNA. J Virol **82:** 11851–11858

Pantaleo V, Rubino L, Russo M (2003) Replication of Carnation Italian ringspot virus defective interfering RNA in Saccharomyces cerevisiae. J Virol **77:** 2116–2123

Pantaleo V, Szittya G, Burgyán J (2007) Molecular bases of viral RNA targeting by viral small interfering RNA-programmed RISC. J Virol **81:** 3797–3806

Parizotto EA, Dunoyer P, Rahm N, Himber C, Voinnet O (2004) In vivo investigation of the transcription, processing, endonucleolytic activity, and functional relevance of the spatial distribution of a plant miRNA. Genes Dev **18:** 2237–2242

Pignatta D, Kumar P, Turina M, Dandekar A, Falk BW (2007) Quantitative analysis of efficient endogenous gene silencing in Nicotiana benthamiana plants using tomato bushy stunt virus vectors that retain the capsid protein gene. Mol Plant Microbe Interact **20:** 609–618

Qiu W, Park JW, Scholthof HB (2002) Tombusvirus P19-mediated suppression of virus-induced gene silencing is controlled by genetic and dosage features that influence pathogenicity. Mol Plant Microbe Interact **15:** 269–280

Rhoades MW, Reinhart BJ, Lim LP, Burge CB, Bartel B, Bartel DP (2002) Prediction of plant microRNA targets. Cell **110:** 513–520

Rubino L, Carrington JC, Russo M (1992) Biologically active cymbidium ringspot virus satellite RNA in transgenic plants suppresses accumulation of DI RNA. Virology **188:** 429–437

Scholthof HB, Alvarado VY, Vega-Arreguin JC, Ciomperlik J, Odokonyero D, Brosseau C, Jaubert M, Zamora A, Moffett P (2011a) Identification of an *ARGONAUTE* for antiviral RNA silencing in *Nicotiana benthamiana*. Plant Physiol **156:** 1548–1555

Scholthof KB, Adkins S, Czosnek H, Palukaitis P, Jacquot E, Hohn T, Hohn B, Saunders K, Candresse T, Ahlquist P, et al (2011b) Top 10 plant viruses in molecular plant pathology. Mol Plant Pathol **12:** 938–954

Schott G, Mari-Ordonez A, Himber C, Alioua A, Voinnet O, Dunoyer P (2012) Differential effects of viral silencing suppressors on siRNA and miRNA loading support the existence of two distinct cellular pools of ARGONAUTE1. EMBO J **31:** 2553–2565

Schuck J, Gursinsky T, Pantaleo V, Burgyán J, Behrens SE (2013) AGO/RISC-mediated antiviral RNA silencing in a plant in vitro system. Nucleic Acids Res **41:** 5090–5103

Shimura H, Pantaleo V, Ishihara T, Myojo N, Inaba J, Sueda K, Burgyán J, Masuta C (2011) A viral satellite RNA induces yellow symptoms on tobacco by targeting a gene involved in chlorophyll biosynthesis using the RNA silencing machinery. PLoS Pathog **7:** e1002021

Sorin C, Bussell JD, Camus I, Ljung K, Kowalczyk M, Geiss G, McKhann H, Garcion C, Vaucheret H, Sandberg G, et al (2005) Auxin and light control of adventitious rooting in *Arabidopsis* require ARGONAUTE1. Plant Cell **17:** 1343–1359

Souret FF, Kastenmayer JP, Green PJ (2004) AtXRN4 degrades mRNA in Arabidopsis and its substrates include selected miRNA targets. Mol Cell **15:** 173–183

Szittya G, Molnár A, Silhavy D, Hornyik C, Burgyán J (2002) Short defective interfering RNAs of tombusviruses are not targeted but trigger post-transcriptional gene silencing against their helper virus. Plant Cell **14:** 359–372

Szittya G, Moxon S, Pantaleo V, Toth G, Rusholme Pilcher RL, Moulton V, Burgyan J, Dalmay T (2010) Structural and functional analysis of viral siRNAs. PLoS Pathog **6:** e1000838

Takeda A, Iwasaki S, Watanabe T, Utsumi M, Watanabe Y (2008) The mechanism selecting the guide strand from small RNA duplexes is different among argonaute proteins. Plant Cell Physiol **49:** 493–500

Thompson JD, Higgins DG, Gibson TJ (1994) CLUSTAL W: improving the sensitivity of progressive multiple sequence alignment through sequence weighting, position-specific gap penalties and weight matrix choice. Nucleic Acids Res **22:** 4673–4680

Várallyay E, Havelda Z (2013) Unrelated viral suppressors of RNA silencing mediate the control of ARGONAUTE1 level. Mol Plant Pathol **14:** 567–575

Várallyay É, Oláh E, Havelda Z (2014) Independent parallel functions of p19 plant viral suppressor of RNA silencing required for effective suppressor activity. Nucleic Acids Res **42:** 599–608

Várallyay E, Válóczi A, Agyi A, Burgyán J, Havelda Z (2010) Plant virus-mediated induction of miR168 is associated with repression of ARGONAUTE1 accumulation. EMBO J **29:** 3507–3519

Vargason JM, Szittya G, Burgyán J, Hall TM (2003) Size selective recognition of siRNA by an RNA silencing suppressor. Cell **115:** 799–811

Vaucheret H (2008) Plant ARGONAUTES. Trends Plant Sci **13:** 350–358

Vaucheret H (2009) AGO1 homeostasis involves differential production of 21-nt and 22-nt miR168 species by MIR168a and MIR168b. PLoS ONE **4:** e6442

Vaucheret H, Mallory AC, Bartel DP (2006) AGO1 homeostasis entails coexpression of MIR168 and AGO1 and preferential stabilization of miR168 by AGO1. Mol Cell **22:** 129–136

Vaucheret H, Vazquez F, Crété P, Bartel DP (2004) The action of ARGONAUTE1 in the miRNA pathway and its regulation by the miRNA pathway are crucial for plant development. Genes Dev **18:** 1187–1197

Vazquez F, Gasciolli V, Crété P, Vaucheret H (2004) The nuclear dsRNA binding protein HYL1 is required for microRNA accumulation and plant development, but not posttranscriptional transgene silencing. Curr Biol **14:** 346–351

Voinnet O, Pinto YM, Baulcombe DC (1999) Suppression of gene silencing: a general strategy used by diverse DNA and RNA viruses of plants. Proc Natl Acad Sci USA **96:** 14147–14152

Wang XB, Jovel J, Udomporn P, Wang Y, Wu Q, Li WX, Gasciolli V, Vaucheret H, Ding SW (2011) The 21-nucleotide, but not 22-nucleotide, viral secondary small interfering RNAs direct potent antiviral defense by two cooperative argonautes in *Arabidopsis thaliana*. Plant Cell **23:** 1625–1638

Yamamura Y, Scholthof HB (2005) Tomato bushy stunt virus: a resilient model system to study virus-plant interactions. Mol Plant Pathol **6:** 491–502

Yu H, Grassmann CW, Behrens SE (1999) Sequence and structural elements at the 3′ terminus of bovine viral diarrhea virus genomic RNA: functional role during RNA replication. J Virol **73:** 3638–3648

Zhang X, Yuan YR, Pei Y, Lin SS, Tuschl T, Patel DJ, Chua NH (2006) Cucumber mosaic virus-encoded 2b suppressor inhibits Arabidopsis Argonaute1 cleavage activity to counter plant defense. Genes Dev **20:** 3255–3268

Zuker M (2003) Mfold web server for nucleic acid folding and hybridization prediction. Nucleic Acids Res **31:** 3406–3415